Available online at www.sciencedirect.com

ScienceDirect

Ceramics International 40 (2014) 4631–4638

CERAMICS INTERNATIONAL

www.elsevier.com/locate/ceramint

Low-temperature synthesis of $BiVO_4$ powders by Pluronic-assisted hydrothermal method: Effect of the surfactant and temperature on the morphology and structural control

U.M. García-Pérez[a,b,*], A. Martínez-de la Cruz[b], S. Sepúlveda-Guzmán[b], J. Peral[c]

[a]Universidad Autónoma de Nuevo León, Facultad de Ingeniería Mecánica y Eléctrica, Centro de Investigación e Innovación en Ingeniería Aeronáutica, Carretera a Salinas Victoria Km 2.3, C.P. 66600 Apodaca, N.L., Mexico

[b]Universidad Autónoma de Nuevo León, Facultad de Ingeniería Mecánica y Eléctrica, Av. Universidad s/n, Ciudad Universitaria, C.P. 66451, San Nicolás de los Garza, N.L., Mexico

[c]Universitat Autònoma de Barcelona, Department de Química, 08193 Cerdanyola del Vallès, Spain

Received 21 July 2013; received in revised form 1 September 2013; accepted 1 September 2013
Available online 7 September 2013

Abstract

$BiVO_4$ photocatalyst was successfully synthesized by the hydrothermal method using Pluronic F-127 as morphology-directing agent. $BiVO_4$ powders with a pure monoclinic phase were obtained at 80 °C. For optimizing the conditions of synthesis and investigate the product formation mechanism, the temperature of synthesis was systematically investigated. The structural and morphological properties of the as-synthesized $BiVO_4$ photocatalysts were characterized by X-ray powder diffraction (XRD), and scanning electron microscopy (SEM). Nitrogen adsorption measurements (BET) were employed to analyze the specific surface area of the samples. The band gap of the as-prepared $BiVO_4$ samples was determined from the onset of the absorption band of UV–vis diffuse reflectance spectra. The quasi-Fermi potential of electrons of the synthesized samples was determined through pH dependent photovoltage measurements. The photocatalytic activities of the as-synthesized catalysts were evaluated in the photodegradation reaction of an aqueous solution of rhodamine B under visible-light irradiation. The mechanism of formation of the as-prepared $BiVO_4$ samples has also been proposed.

Keywords: Semiconductors; $BiVO_4$; Hydrothermal synthesis; X-ray diffraction; Photocatalysis

1. Introduction

Since the contributions made by Fujishima and Honda to the photoelectrochemistry field with the hydrogen production by photoelectrochemical splitting of water on n-type TiO_2 electrodes under UV-irradiation [1], many researchers have focused their attention on the development of novel visible-light-driven semiconductor materials.

Recently, the photochemistry of transition-metal oxides has received the attention for environmental (water purification) and energy (hydrogen production) applications. Some materials, such as Bi_2WO_6, $AgVO_3$, Ag_3VO_4, $CuWO_4$ and $BiVO_4$ have demonstrated their potential in the heterogeneous photocatalysis field when were used as photocatalysts for removing organic contaminants from water (dyes, pesticides, volatile organic compounds, etc.) or for the splitting of water into hydrogen and oxygen under UV or visible-light irradiation [2–8]. Among these photocatalysts, $BiVO_4$ with monoclinic structure and a discrete band gap of ca. 2.3 eV, have proven to be a suitable visible-light photocatalyst for the photocatalytic degradation of harmful pollutants and oxygen evolution from an aqueous $AgNO_3$ solution [9].

It is well-known that photocatalytic activity closely relates to powder catalyst properties like particle size, specific surface area, crystallinity, crystal structure, crystalline orientation, surface purity, etc. Consequently, intensive efforts have been made in order to develop new routes for the controlled synthesis of $BiVO_4$ powders. A common strategy for the

*Corresponding author at: Universidad Autónoma de Nuevo León, Facultad de Ingeniería Mecánica y Eléctrica, Centro de Investigación e Innovación en Ingeniería Aeronáutica, Carretera a Salinas Victoria Km 2.3, C.P. 66600 Apodaca, N.L., Mexico. Tel.: +52 81 83294020; fax: +52 81 83320903.
E-mail address: ulisesma.garcia@gmail.com (U.M. García-Pérez).

0272-8842/$ - see front matter © 2013 Elsevier Ltd and Techna Group S.r.l. All rights reserved.
http://dx.doi.org/10.1016/j.ceramint.2013.09.002

tuning and control of the morphologies and sizes of particles has been the use of surfactants, polymers or organic compounds as morphology-directing templates. In our previous works [10–12], we have synthesized monoclinic $BiVO_4$ particles with spherical shape and spherical-shaped self-assembled structures by a simple combustion synthesis method, by hydrothermal treatment, and by a co-precipitation method, using sodium carboxymethylcellulose and Pluronic P-123 as morphology-directing agents.

Recently, Meng et al. used a hydrothermal process with Pluronic P-123 as a soft template to fabricate crystalline monoclinic $BiVO_4$ powders with polyhedral, rod-like, tubular, leaf-like and spherical morphologies at different pH values [13].

In the present study, monoclinic $BiVO_4$ powders were synthesized by a facile Pluronic-assisted hydrothermal method at low temperatures. Polyethylene oxide/polypropylene oxide/polyethylene oxide ($PEO_{100}PPO_{65}PEO_{100}$) triblock copolymer (Pluronic F-127) was used as agent for the morphology control. The influence of the preparation parameters like hydrothermal temperature and presence of surfactant on the controlled synthesis and the morphology properties of $BiVO_4$ have been discussed. The photocatalytic activities of as-prepared $BiVO_4$ samples were evaluated by the degradation of rhodamine B (rhB) under visible-light irradiation. Moreover, the morphology evolution and the mechanism of formation have also been discussed.

2. Experimental

2.1. Sample preparation

Crystalline $BiVO_4$ powders were synthesized by the Pluronic-assisted hydrothermal method. All chemicals used were obtained from commercial sources as analytical reagents. A typical synthesis process is as follows: 0.03 mol of Bi $(NO_3)_3 \cdot 5H_2O$ (Aldrich, 99%) and 0.03 mol of NH_4VO_3 (Productos Químicos Monterrey, 99%) were dissolved in 100 mL of a 4 M HNO_3 solution and 100 mL of a 2 M NH_4OH solution at 70 °C, respectively. Meanwhile, 0.58 g of Pluronic F-127 (F-127) was dissolved in 50 mL of distilled water at room temperature. Then 25 mL of F-127 solution was added to each of the Bi and V precursor solutions under vigorous stirring during 1 h to obtain two transparent solutions: A (Bi solution) and B (V solution). Afterwards, solution A was added to solution B under vigorous stirring. The pH of the above mixture was adjusted to 7 with an ammonia solution. Then the mixture was stirred for 1 h at room temperature. Afterwards, the yellow suspension obtained was transferred into a 600-mL Teflon-lined stainless steel autoclave and maintained at different temperatures for 20 h under continuous mechanical stirring. The autoclave was then cooled to room temperature. The obtained yellow powders were filtered and washed several times with distilled water and ethanol. Finally, the powders were dried in air for 24 h at 90 °C. The series samples synthesized under various conditions were named as HF, as described in Table 1.

Table 1
Crystal structure, BET surface area and band gap of m-$BiVO_4$ samples synthesized by the surfactant-assisted hydrothermal method at different temperatures during 20 h.

Sample	Temperature ?(°C)	Crystal ?structure	S_{BET} ($m^2\ g^{-1}$)	E_g ?(eV)
HF-60	60	m-s+t-z	ND	ND
HF-80	80	m-s	3.87	2.54
HF-100	100	m-s	6.42	2.53
HF-120	120	m-s	5.97	2.56
HF-140	140	m-s+t-z	ND	ND
HF-160	160	m-s+t-z	ND	ND
HF-180	180	m-s+t-z	ND	ND

m-s: Monoclinic scheelite; t-z: tetragonal zircon; ND: non-determined.

2.2. Sample characterization

The phase transitions of the as-synthesized samples were studied by X-ray powder diffraction using a Bruker D8 Advanced diffractometer with Cu K_α radiation coupled with a Vantec high speed detector and Ni filters. The detection range was from 10° to 70° with a step size of 0.05°. The morphology of the as-prepared samples was investigated by field-emission scanning electron microscope (FE-SEM, FEI Nova Nanosem 200). The Brunauer–Emmett–Teller (BET) surface areas of the samples were determined by nitrogen adsorption measurements using a Bel-Japan Minisorp II surface area and pore size analyzer. The adsorption–desorption isotherms were evaluated at −196 °C after the samples were degassed at 80 °C for 24 h. Optical absorption spectra of the samples were obtained using an UV–visible spectrophotometer (Perkin-Elmer Precisely Lambda 35) equipped with an integrating sphere. UV–vis diffuse reflectance spectra (DRS) of $BiVO_4$ were recorded by using $BaSO_4$ as a reference. Quasi-Fermi levels of electrons ($_nE_F^*$) were measured according to a procedure described elsewhere [6]. Briefly, 80 mg of HF-samples was suspended in 80 mL of 0.1 M KNO_3 in the presence of 6 mg of methylviologen dichloride (MV^{2+}) and irradiated with visible light ($\lambda \geq 390$ nm, four compact fluorescent lamps of 15 W were used as light source). Suspensions were stirred and bubbled with N_2 prior to and during the measurement. The pH was adjusted with HNO_3 (1 M) and NaOH (0.001 M, 0.01 M, 0.05 M, 0.1 M and 1 M) solutions and monitored with a pH-meter. A platinum plate (1 cm^2) and a saturated calomel (SCE) were used as working and reference electrodes, respectively. Stable photovoltages were recorded 30 min after adjusting the pH value. Those values were plotted as a function of pH, and the pH_0 values obtained from the inflection points were converted to the quasi-Fermi potential of electrons at pH 0 by the equation:

$$_nE_F(pH_0) = E^0_{MV^{2+/+}} - k(0 - pH_0) \quad (1)$$

where E^0 is the standard reduction potential of the redox couple (−0.445 V vs. NHE), and k is a constant for each specific material. A k-value of 0.054 V/pH has been previously calculated by Long et al. for powders of $BiVO_4$ [14].

2.3. Photocatalytic reactions

Photocatalytic activities of the as-prepared samples were evaluated by degradation of rhB under visible-light irradiation of a Xe lamp of 6000 K with an illuminance of 1630 lx. In each experiment, 0.250 g of photocatalyst was added into 250 mL of rhB solution (5 mg/L). Afterwards, the suspension was put in an ultrasonic bath for 10 min to eliminate aggregates. Prior illumination, the suspensions were magnetically stirred in the dark for 1 h to ensure the establishment of adsorption–desorption equilibrium between the photocatalyst and the dye. The photocatalytic experiments were carried out at 25 ± 1 °C. Six milliliters samples were taken at different intervals of time and centrifuged to remove the photocatalyst particles. Then, the rhB concentration was determined through its absorption at 554 nm by using a UV–vis spectrophotometer (Perkin-Elmer Lambda 35).

3. Results and discussions

3.1. Structural characterization

Fig. 1 shows the XRD patterns of the as-prepared samples by the Pluronic-assisted hydrothermal method. For $BiVO_4$ as-synthesized at 60 °C (Fig. 1b), the pattern shows that the powders crystallized as a mixture of tetragonal (JCPDS 14-0133) and monoclinic (JCPDS 14-0688) phase. As the temperature increases to 80 °C (Fig. 1c), the peaks indicate that the sample is well crystallized in the pure monoclinic phase. For the samples prepared at 100 °C and 120 °C (Fig. 1d, e), all diffraction peaks can be assigned to the pure monoclinic structure. As the temperature increases to 140 °C, 160 °C and 180 °C (Fig. 1f–h), the peaks for the tetragonal phase begin to appear, indicating that a mixture of monoclinic and tetragonal phase of $BiVO_4$ coexists. The results suggest that the temperature of synthesis is an important factor in preparing pure monoclinic $BiVO_4$. In order to determine the influence of an additive in the synthesis of monoclinic $BiVO_4$ at low temperature (80 °C) the same procedure of synthesis was carried out without the presence of Pluronic F-127 (Fig. 1i). The XRD pattern obtained does not show the presence of diffraction lines associated to the tetragonal and monoclinic phase. This result evidences the role played by the additive in the selective synthesis of crystalline $BiVO_4$ particles with monoclinic structure at low temperatures following a hydrothermal method.

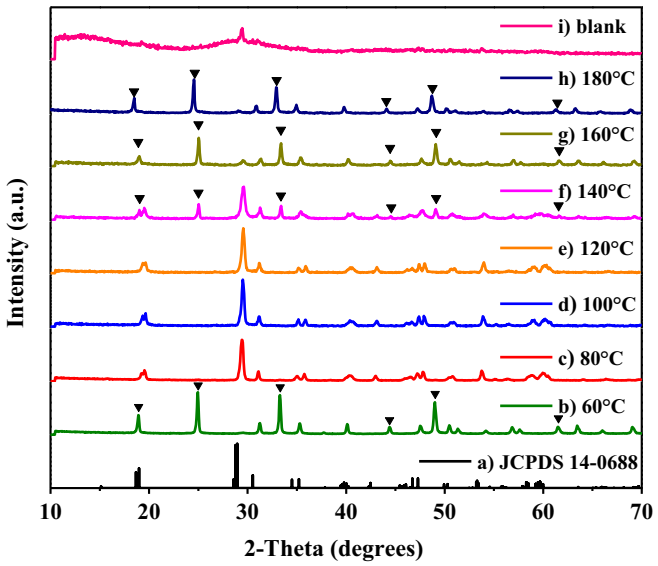

Fig. 1. XRD patterns of samples prepared by the surfactant-assisted hydrothermal method at different temperatures during 20 h: (a) standard XRD pattern of m-$BiVO_4$ (JCPDS no. 14-0688), (b) 60 °C, (c) 80 °C, (d) 100 °C, (e) 120 °C, (f) 140 °C, (g) 160 °C, (h) 180 °C, and (i) 80 °C without additive.

3.2. Morphology characterization

Fig. 2 shows the SEM images obtained for the samples prepared by the Pluronic-assisted hydrothermal method at different temperatures during 20 h. For $BiVO_4$ powders synthesized at 80 °C (Fig. 2a, b), the images indicate that the morphology of the particles is composed by 3-D arrays of particles with a dendrite-like morphology with unidirectional growth. The images demonstrate the length of the trunks is 1.5–2.5 μm; while the length of the branches ranges from 500 nm to 1 μm. These results show that it was possible to synthesize pure monoclinic phase of $BiVO_4$ with dendrite morphology at low temperatures and neutral pH, which is a different result than that reported by other research groups, where particles with this type of 3-D arrays of pure phase monoclinic $BiVO_4$ powders obtained by hydrothermal methods in the absence or presence of organic additives, were only obtained in acid or basic conditions of reaction and elevated temperatures ranging from 120 °C to 200 °C [13,15–18]. In recent studies, researchers have reported the hydrothermal synthesis of $BiVO_4$ powders with dendritic morphology at similar temperatures (80 °C), but with longer reaction times (30 h) and more aggressive reaction conditions (pH=3) [19].

Fig. 2c–f is the images of the powders prepared at 100 °C and 120 °C. As seen, they consist of well-separated semispherical nanoparticles with an average size of about 60 nm and nanorods with a diameter and length about 60 nm and 50 nm, respectively. These results reveal that the temperature of the hydrothermal synthesis was an important factor for controlling the morphologies of $BiVO_4$ particles synthesized by the Pluronic-assisted hydrothermal method.

A possible formation mechanism of m-$BiVO_4$ particles synthesized by Pluronic-assisted hydrothermal process is described in Fig. 3. The m-$BiVO_4$ formation was a typical hydrothermal ripening process. At the beginning, BiO^+ and VO_3^- ions are dissolved in the presence of Pluronic F-127 molecules separately. The BiO^+ ions are bond to the surfactant as a consequence of the electrostatic interactions between ions and terminal groups (–OH) of the hydrophilic part of surfactant molecules. Meanwhile, VO_3^- ions are dissolved with a limited diffusion due to the steric effect of surfactant molecules. In addition is experimenting electrostatic repulsion due to the negative charge of both species.

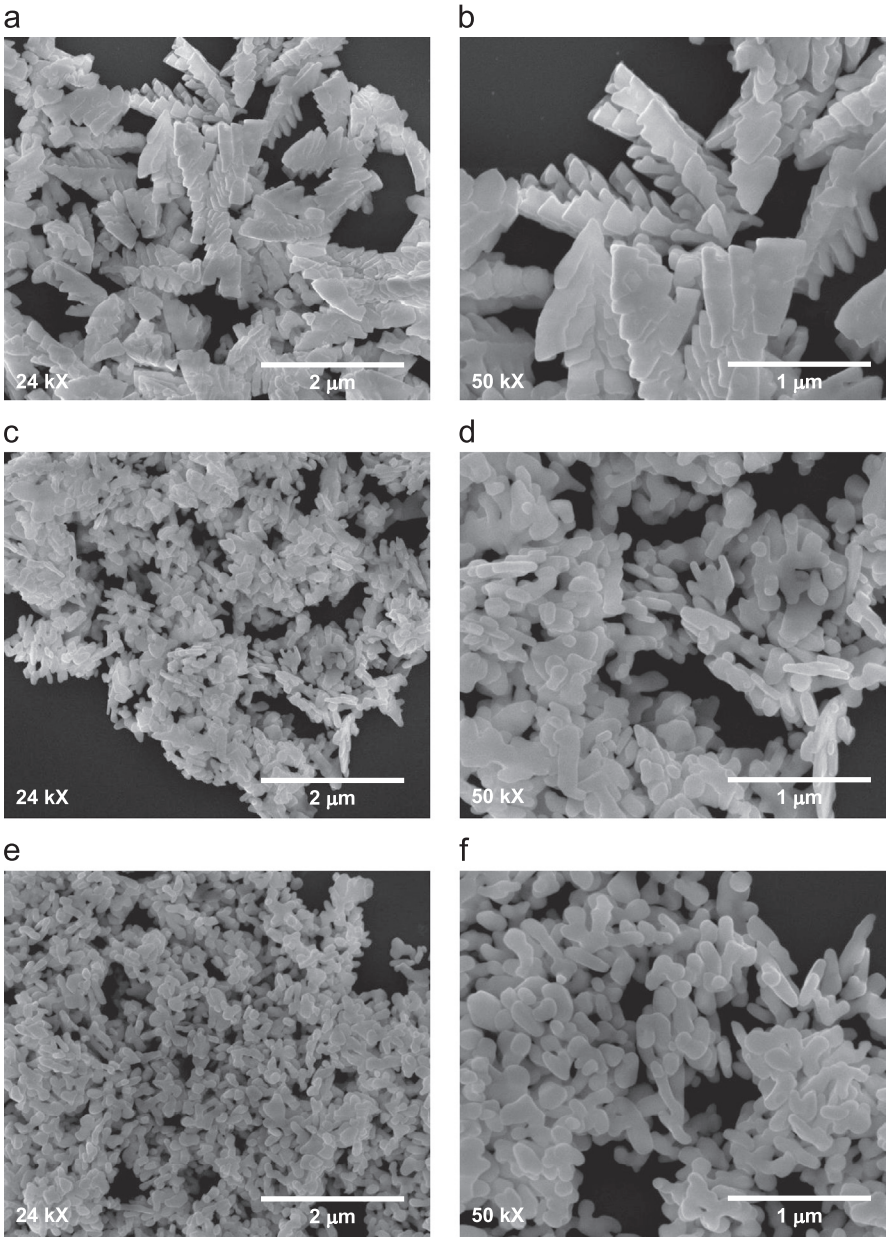

Fig. 2. SEM images of m-$BiVO_4$ powders synthesized by the surfactant-assisted hydrothermal method at different temperatures during 20 h: (a, b) 80 °C, (c, d) 100 °C, and (e, f) 120 °C.

It is well known that the Pluronic F-127 is a nonionic surfactant, which has a relatively high critical micelle concentration (CMC) due to the low hydrophobicity of PPO blocks, 0.8 wt% at room temperature [20]. Hence, it is possible to say that due to the low concentration used in the synthesis of materials is not possible to carry out the formation of micelles in aqueous solution because the concentration employed is below the CMC of the VO_3^- surfactant. According to the proposed mechanism, the addition of ions into the bismuth nitrate solution permit the formation of tiny crystalline nuclei. In this stage, the Pluronic F-127 plays a very important role in the controlled growth of the nuclei because it acts as steric stabilizer. During the hydrothermal treatment at low temperature (80 °C), it can be seen that the aggregated particles grow with a preferential orientation. This aggregation of particles can be explained due to their high surface energy, which can be stabilized by the adsorption of the organic molecules or ammonium radicals. Recently, the preferential growth of m-$BiVO_4$ along the [100] or [010] directions has been also observed by other researchers [15,21–23].

The effect of higher hydrothermal temperatures (100 °C and 120 °C) on the growth mechanism and morphologies of the products can be explained on the basis of the dissolution–recrystallization mechanism, in which the particles aggregated and crystallized at 80 °C gradually dissolve and recrystallize giving the crystal growth. The larger particles grew at the cost of the small ones, due to the energy difference in solubility between the large particles and the smaller particles, according to the well-known

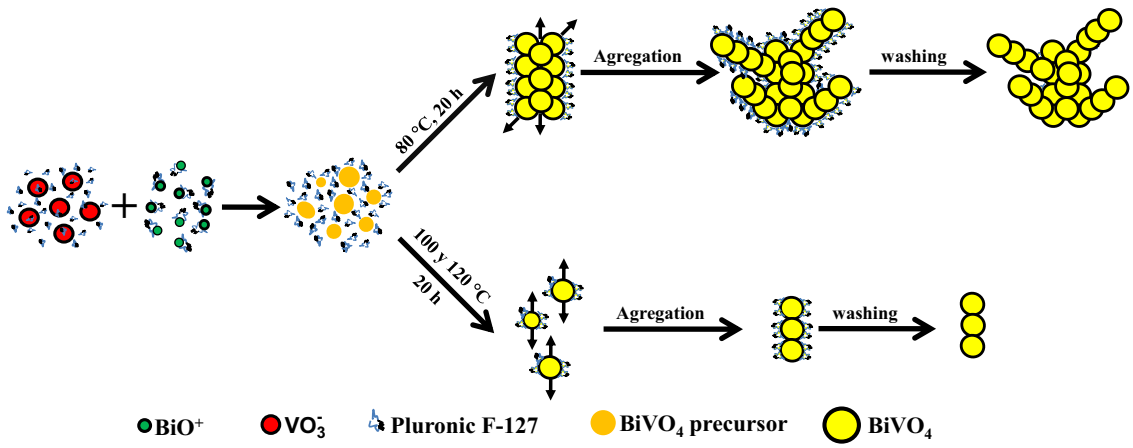

Fig. 3. Schematic illustration of the mechanism of formation of the as-prepared m-$BiVO_4$ samples by the Pluronic-assisted hydrothermal method.

Gibbs–Thomson law [24]. Thus, the monoclinic phase $BiVO_4$ nuclei were generated to form semispherical nanoparticles. A similar growth mechanism has been reported by Zhou et al. when they synthesized single-crystalline $BiVO_4$ microtubes with square cross-sections via a reflux method [21].

3.3. Specific surface area and UV–vis diffuse absorption spectra analysis

The BET specific surface area (S_{BET}) of the HF samples was calculated from N_2 isotherms at −196.68 °C. As shown in Table 1, the surface area values increase from 3.87 to 5.97 $m^2\,g^{-1}$ when the temperature increases from 80 °C to 120 °C, which agrees the fact that particle size is reduced with temperature in the range of 80–120 °C. The S_{BET} values obtained in this work for m-$BiVO_4$ powders synthesized by the hydrothermal route in the presence of Pluronic F-127 showed that it is possible to obtain powders with a surface area greater than those reported in the literature for materials that have been synthesized by the hydrothermal method in the absence or presence of other additives, such as CTAB or glucose. [18,22,25–27].

UV–visible diffuse reflectance spectra were obtained for the pure monoclinic phase samples prepared by the Pluronic-assisted hydrothermal method (data not shown). The spectra demonstrate that all the HF samples had a high photoabsorption capacity of UV and visible light up to 510 nm, suggesting their potential photocatalytic activity under visible light. The color of the samples was yellow, which is in accordance with the absorption band edge at 510 nm. The obtained band gap energies (E_g) for the HF samples are listed in Table 1. The E_g of the samples were estimated in the range of 2.54–2.56 eV from the onset of the absorption edge, which are similar to the values previously reported for $BiVO_4$ oxide with monoclinic structure [28,29].

3.4. Photoelectrochemical characterization

The position of the quasi-Fermi level of electrons ($_nE_F^*$) in the pure monoclinic $BiVO_4$ samples synthesized by the Pluronic-assisted hydrothermal method was determined measuring the photovoltage of a dispersion of the photocatalyst in presence of MV^{2+} at different pH. Fig. 4 can help to visualize the effect of pH on the photovoltage developed on m-$BiVO_4$ suspensions under visible-light irradiation. Due to the specific features of the redox processes that involve the semiconductor particles, the position of their energy bands changes with pH, while the redox potential of the MV^{2+}/MV^{+} couple is pH independent. Thus, by changing the pH, the photoassisted charge transfer between the catalyst and the redox couple can be changed, and this affects the photovoltage developed by the particles. In particular, when $_nE_F^*$ in the solid becomes equal to the redox potential of the MV^{2+}/MV^{+} couple a large photovoltage change is noticed due to the disappearance of charge transfer. This is seen in the photovoltage vs. pH curve as a clear inflection point that can be used to characterize $_nE_F^*$. The pH values of the inflection points (pH_0) were 10.39 (HF-80), 10.30 (HF-100) and 11.56 (HF-120). The quasi-Fermi levels of electrons obtained at pH 0 by using Eq. (1) were 0.11 V, 0.13 V and 0.17 V for the samples synthesized at 80 °C, 100 °C and 120 °C, respectively. Accordingly, reduction of water is thermodynamically not allowed with these materials.

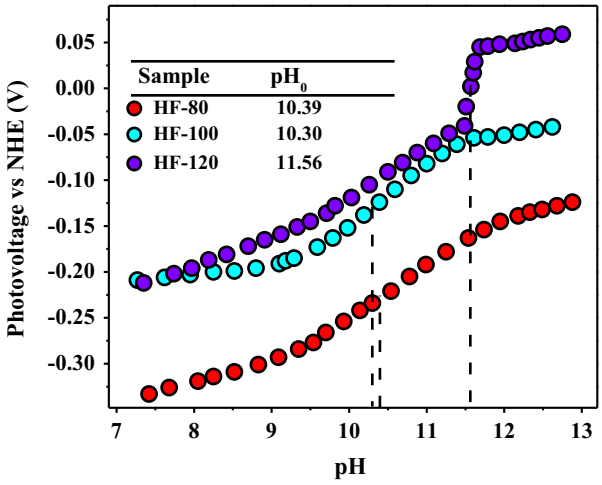

Fig. 4. Variation of voltage with pH for a suspension of m-$BiVO_4$ powders in 0.1 M KNO_3 in the presence of MV^{2+} under visible-light irradiation ($\lambda \geq 390$ nm).

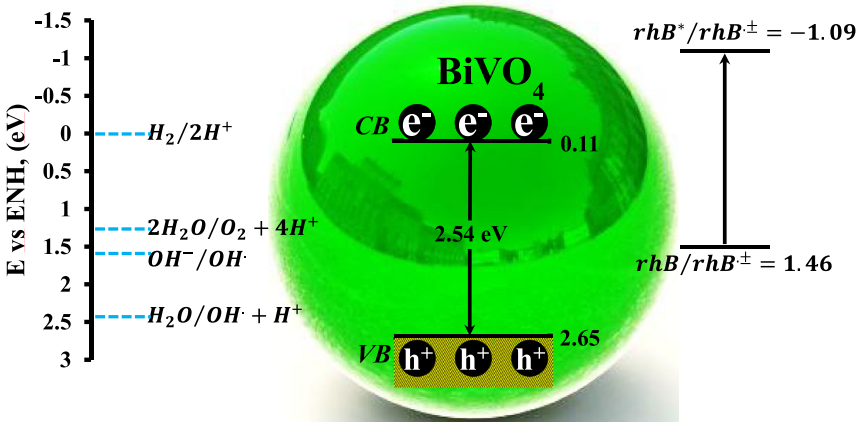

Fig. 5. Diagram of band energy position of $BiVO_4$ and redox potentials of selected couples.

The results obtained are close to the previous values reported by our group and by Kisch et al. [12,14]. The difference between the values can be attributed to differences in crystallinity [30], due to the different methods of synthesis used to obtain the oxide.

Knowing the quasi-Fermi level of electrons also allows the estimation of the valence band and the holes energy. The valence band edge positions of the samples synthesized at 80 °C, 100 °C and 120 °C were located at 2.65 V, 2.67 V and 2.72 V, respectively. Fig. 5 shows that these values of hole energy make feasible the oxidation of water to oxygen.

In addition, due to the relative positions at pH 0 of the standard redox potential of the dye $E^0 rhB/rhB^{\pm} = 1.46$ V vs. NHE and $(E^0 rhB^*/rhB^+) = -1.09$ V vs. NHE [31], it is possible to conclude that an electron transfer from the adsorbed rhB in its singlet excited state to the conduction band of m-$BiVO_4$ samples is possible and thus, the excited dye could be oxidized by the semiconductor. On the other hand, the conduction band electron can, by reduction of dissolved oxygen, generate powerful oxidizing agents (superoxide radical anion, O_2^-, and hydroxyl radical, $\cdot OH$) that can further degrade the dye molecule.

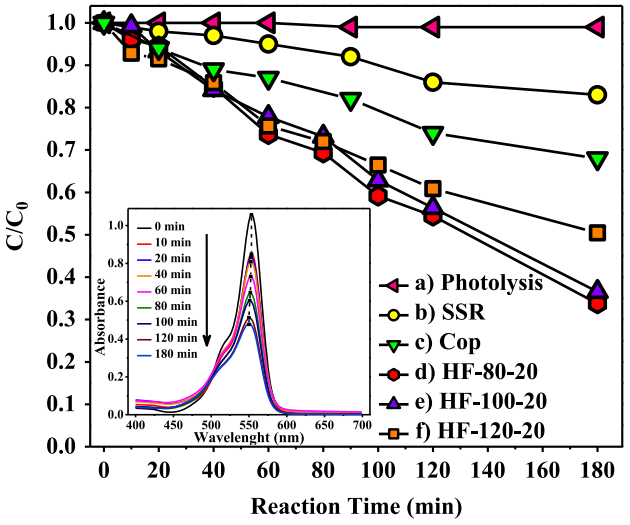

Fig. 6. Change in the rhB concentration during its photocatalytic degradation in the presence of m-$BiVO_4$ samples. The inset includes the temporal evolution of the spectral changes taking place during the photodegradation of rhB by using as photocatalyst the H-80 sample.

3.5. Photocatalytic reactions

The photocatalytic behavior of the HF samples synthesized by the Pluronic-assisted hydrothermal method was investigated on the photodegradation of rhB under visible-light irradiation. Fig. 6 shows the evolution of the dye concentration during the irradiation of the photocatalytic system. For determining the natural degradation (photolysis) of the dye under visible-light irradiation a blank test was realized in absence of the photocalyst. The curve obtained (Fig. 6a) shows that the dye solution was stable after 180 min of light irradiation. In order to compare the photoactivity of the materials synthesized in the present work, the photodegradation of the dye in solution was also evaluated by using $BiVO_4$ oxides synthesized by solid-state reaction and by co-precipitation. The curves obtained for those reference materials showed a decolorization of the dye solution of 17% (Fig. 6b) and 32% (Fig. 6c), respectively. A noticeable increase of the photocatalytic activity was observed with the HF samples. Fig. 6d shows that for the HF-80 sample the photodegradation rate is over 67% after 180 min of visible-light irradiation, while for the HF-100 and HF-120 samples it was over 64% and 50%, respectively.

The kinetic parameters of the photocatalytic reactions of the samples synthesized by the hydrothermal method were evaluated using the data shown in Fig. 6. The data of the material prepared at 80 °C (H-80) and 100 °C (H-100) can be adjusted to fit a zero-order rate reaction. On the other hand, the degradation of rhB using as photocatalyst the sample H-120 and the reference materials followed a first-order rate reaction. On the basis of these models, the half-life times for bleaching of the rhB solutions under visible-light irradiation were 693 min (SSR), 267 min (Cop), 132 min (H-80), 139 min (H-100), and 174 min (H-120). Therefore, the sample H-80 was the material with a better photocatalytic performance.

The results obtained show that the photocatalytic activity of the materials is not in correlation with surface area. Generally,

the activity of a photocatalyst increases with an increase in surface area, not only because the photocatalytic reaction usually takes place on the surface, but also because the efficiency of the electron–hole separation is improved. However, other factors, such as crystallinity and crystal structure, particle size, crystalline orientation, and purity on the surface particles, have an important role to play in the improvement of the photocatalytic properties of the semiconductor materials due to their influence in the efficiency of the electron–hole separation [32].

In order to gain knowledge about the mechanism of photodegradation of the dye the temporal evolution of the spectral changes taking place during the photodegradation of rhB was studied by using as photocatalyst the sample H-80 (inset in Fig. 6). As illustrated, the dye has a main rhB absorption band located at 554 nm, which is due to the presence of four ethyl groups on the molecule dye. It is well known that rhB degradation occurs via two competitive processes, N-dealkylation and the destruction of the conjugated structure [33]. The reduction of the absorption band of the rhB solution at 554 nm corresponds to the decomposition of the conjugated xanthene ring in rhB. The absorption band shift of the rhB solution toward the blue region suggests the formation of de-ethylated rhB molecules [34].

In the case of the H-80 sample, after 180 min of visible light irradiation it is possible to observe that the main rhB absorption band gradually shifts from 554 nm to 500 nm, demonstrating that rhB degrades by following the de-ethylation degradation mechanism. The gradual peak wavelength shifting toward the blue region confirms that ethyl groups are sequentially removed, something that is in accordance with similar hypsochromic shifts seen by Ren et al. for the rhB/$BiVO_4$ system [29].

4. Conclusions

Pure $BiVO_4$ powders with monoclinic structure were selectively synthesized by a facile Pluronic-assisted hydrothermal method. The presence of Pluronic F-127 and hydrothermal temperature have a significant influence in the controllable synthesis and morphology of the obtained $BiVO_4$ powders. $BiVO_4$ with a regular hyperbranched structure and pure monoclinic phase can be obtained at a lower hydrothermal temperature (80 °C). The as-prepared $BiVO_4$ with a 3-D structure exhibits a better photocatalytic activity for the degradation of rhB than the semispherical nanoparticles of the reference materials.

Acknowledgments

The authors acknowledge the financial support provided by the CONACYT (Grants nos. 178895 and 167018), the SEP-PROMEP (Grant no. UANL-PTC-590), the PAICYT (Grant no. IT715-11) and the Spanish "Ministerio de Ciencia e Innovación" (CTQ 2008-00178 Project).

References

[1] A. Fujishima, K. Honda, Electrochemical photolysis of water at a semiconductor electrode, Nature 238 (1972) 37.
[2] C.Y. Wang, H. Zhang, F. Li, L. Zhu, Degradation and mineralization of Bisphenol A by mesoporous Bi_2WO_6 under simulated solar light irradiation, Environmental Science and Technology 44 (2010) 6843.
[3] G.P. Nagabhushana, G. Nagaraju, G.T. Chandrappa, Synthesis of bismuth vanadate: its application in H_2 evolution and sunlight-driven photodegradation, Journal of Materials Chemistry A 1 (2013) 388.
[4] R. Konta, H. Kato, H. Kobayashi, A. Kudo, Photophysical properties and photocatalytic activities under visible light irradiation of silver vanadates, Physical Chemistry Chemical Physics 5 (2003) 3061.
[5] C.M. Huang, G.T. Pan, Y.C.M. Li, M.H. Li, T.C.K. Yang, Crystalline phases and photocatalytic activities of hydrothermal synthesis Ag_3VO_4 and $Ag_4V_2O_7$ under visible light irradiation, Applied Catalysis A: General 358 (2009) 164.
[6] U.M. García-Pérez, A. Martínez-de la Cruz, J. Peral, Transition metal tungstates synthesized by co-precipitation method: basic photocatalytic properties, Electrochimica Acta 81 (2012) 227.
[7] S. Obregón, A. Caballero, G. Colón, Hydrothermal synthesis of $BiVO_4$: structural and morphological influence on the photocatalytic activity, Applied Catalysis B: Environmental 117–118 (2012) 59.
[8] A. Martínez-de la Cruz, U.M. García Pérez, Photocatalytic properties of $BiVO_4$ prepared by the co-precipitation method: degradation of rhodamine B and possible reaction mechanisms under visible irradiation, Materials Research Bulletin 45 (2010) 135–141.
[9] G. Xi, J. Ye, Synthesis of bismuth vanadate nanoplates with exposed {001} facets and enhanced visible-light photocatalytic properties, Chemical Communications 46 (2010) 1893.
[10] U.M. García Pérez, S. Sepúlveda-Guzmán, A. Martínez-de la Cruz, U. Ortiz Méndez, Photocatalytic activity of $BiVO_4$ nanospheres obtained by solution combustion synthesis using sodium carboxymethylcellulose, Journal of Molecular Catalysis A: Chemical 335 (2011) 169.
[11] A. Martínez-de la Cruz, U.M. García-Pérez, S. Sepúlveda-Guzmán, Characterization of the visible-light-driven $BiVO_4$ photocatalyst synthesized via a polymer-assisted hydrothermal method, Research on Chemical Intermediates 39 (2013) 881.
[12] U.M. García-Pérez, S. Sepúlveda-Guzmán, A. Martínez- de la Cruz, J. Peral, Selective synthesis of monoclinic bismuth vanadate powders by surfactant-assisted co-precipitation method: Study of their electrochemical and photocatalytic properties, International Journal of Electrochemical Science 7 (2012) 9622.
[13] X. Meng, L. Zhang, H. Dai, Z. Zhao, R. Zhang, Y. Liu, Surfactant-assisted hydrothermal fabrication and visible-light-driven photocatalytic degradation of methylene blue over multiple morphological $BiVO_4$ single-crystallites, Materials Chemistry and Physics 125 (2011) 59.
[14] M. Long, W. Cai, H. Kisch, Visible light induced photoelectrochemical properties of n-$BiVO_4$ and n-$BiVO_4$/p-Co_3O_4, The Journal of Physical Chemistry C 112 (2008) 548.
[15] Y. Zhao, Y. Xie, X. Zhu, S. Yan, S. Wang, Surfactant-free synthesis of hyperbranched monoclinic bismuth vanadate and its applications in photocatalysis, gas sensing, and lithium-ion batteries, Chemistry: A European Journal 14 (2008) 1601.
[16] Y. Zheng, J. Wu, F. Duan, Y. Xie, Gemini surfactant directed preparation and photocatalysis of m-$BiVO_4$ hierarchical frameworks, Chemistry Letters 36 (2007) 520.
[17] Y. Guo, X. Yang, F. Ma, K. Li, L. Xu, X. Yuan, Y. Guo, Additive-free controllable fabrication of bismuth vanadates and their photocatalytic activity toward dye degradation, Applied Surface Science 256 (2010) 2215.
[18] X. Zhang, Z. Ai, F. Jia, L. Zhang, X. Fan, Z. Zou, Selective synthesis and visible light photocatalytic activities of $BiVO_4$ with different crystaline phases, Materials Chemistry and Physics 103 (2007) 162.
[19] L. Zhou, W. Wang, H. Xu, Controllable synthesis of three-dimensional well-defined $BiVO_4$ mesocrystals via a facile additive-free aqueous strategy, Crystal Growth and Design 8 (2008) 728.

[20] Y. Zhang, Y.M. Lam, Controlled synthesis and association behavior of graft Pluronic in aqueous solutions, Journal of Colloid and Interface Science 306 (2007) 398.
[21] L. Zhou, W. Wang, L. Zhang, H. Xu, W. Zhu, Single-crystalline $BiVO_4$ microtubes with square cross-sections: microstructure, growth mechanism, and photocatalytic property, The Journal of Physical Chemistry C 11 (2007) 13659.
[22] D. Ke, T. Peng, L. Ma, P. Cai, K. Dai, Effects of hydrothermal temperature on the microstructures of $BiVO_4$ and its photocatalytic O_2 evolution activity under visible light, Inorganic Chemistry 48 (2009) 4685.
[23] L. Zhang, D. Chen, X. Jiao, Monoclinic structured $BiVO_4$ nanosheets: hydrothermal preparation, formation mechanism, and coloristic and photocatalytic properties, The Journal of Physical Chemistry B 110 (2006) 2668.
[24] J.W. Mullin, Crystallization, 3rd ed., Butterworth-Heinemaan: Oxford, U.K., 1997.
[25] W. Yin, W. Wang, M. Shang, L. Zhou, S. Sun, L. Wang, $BiVO_4$ Hollow nanospheres anchoring synthesis, growth mechanism, and their application in photocatalysis, European Journal of Inorganic Chemistry 2009 (2009) 4379.
[26] J. Yu, A. Kudo, Effects of structural variation on the photocatalytic performance of hydrothermally synthesized $BiVO_4$, Advanced Functional Materials 16 (2006) 2163.
[27] A. Zhang, J. Zhang, N. Cui, X. Tie, Y. An, L. Li, Effects of pH on hydrothermal synthesis and characterization of visible-light-driven $BiVO_4$ photocatalyst, Journal of Molecular Catalysis A: Chemical 304 (2009) 28.
[28] L. Ren, L. Jin, J.B. Wang, F. Yang, M.Q. Qiu, Y. Yu, Template-free synthesis of $BiVO_4$ nanostructures: I. Nanotubes with hexagonal cross sections by oriented attachment and their photocatalytic property for water splitting under visible light, Nanotechnology 20 (2009) 115603.
[29] L. Ren, L. Ma, L. Jin, J.B. Wang, M. Qiu, Y. Yu, Template-free synthesis of $BiVO_4$ nanostructures: II. Relationship between various microstructures for monoclinic $BiVO_4$ and their photocatalytic activity for the degradation of rhodamine B under visible light, Nanotechnology 20 (2009) 405602.
[30] A. Di Paola, M. Bellardita, R. Ceccato, L. Palmisano, F. Parrino, Highly active photocatalytic TiO_2 powders obtained by thermohydrolysis of $TiCl_4$ in water, The Journal of Physical Chemistry C 113 (2009) 15166.
[31] T. Watanabe, T. Takirawa, K. Honda, Photocatalysis through excitation of adsorbates. 1. Highly efficient N-deethylation of Rhodamine B adsorbed to CdS, The Journal of Physical Chemistry 81 (1977) 1845.
[32] X. Chen, S. Shen, L. Guo, S.S. Mao, Semiconductor-based photocatalytic hydrogen generation, Chemical Reviews 110 (2010) 6503.
[33] C. Chen, X. Li, W. Ma, J. Zhao, H. Hidaka, N. Serpone, Effect of transition metal ions on the TiO_2-assisted photodegradation of dyes under visible irradiation: a probe for the interfacial electron transfer process and reaction mechanism, The Journal of Physical Chemistry B 106 (2002) 318.
[34] J. Wu, F. Duan, Y. Zheng, Y. Xie, Synthesis of Bi_2WO_6 nanoplate-built hierarchical nest-like structures with visible-light-induced photocatalytic activity, The Journal of Physical Chemistry C 111 (2007) 12866.